Effect of chemical composition on mechanical properties and shear band propagation in fully-amorphous ZrCu/ZrCuAl nanolaminates

Cristiano Poltronieri, Andrea Brognara, Chanwon Jung, Fatiha Challali, Philippe Djemia, Gerhard Dehm, James Best, Matteo Ghidelli

Effect of chemical composition on mechanical properties and shear band propagation in fully-amorphous ZrCu/ZrCuAl nanolaminates

C. Poltronieri[1,a], A. Brognara[2], C. Jung[2,b], F. Challali[1], P. Djemia[1], G. Dehm[2], J.P. Best[2], M. Ghidelli[1,*]

[1]Laboratoire des Sciences des Procédés et des Matériaux (LSPM), CNRS, Université Sorbonne Paris Nord, 93430, Villetaneuse, France

[2]Max Planck Institute for Sustainable Materials, 40237 Düsseldorf, Germany

[a]Current address: Carl Zeiss S.p.A., Via Varesina 162, 20156 Milan, Italy

[b]Current address: Department of Materials Science and Engineering, Pukyong National University, 48513 Busan, Republic of Korea

*corresponding author: matteo.ghidelli@lspm.cnrs.fr

Abstract

The mechanical behavior and propagation of shear bands (SBs) in fully amorphous ZrCu/$ZrCuAl_9$ nanolaminates with different nanoscale bilayer period (Λ, from 200 down to 50 nm) was investigated. The combined effect of local chemistry variation and nanointerface density influences the propagation of SBs and the mechanical behavior, reporting nanoindentation hardness values above the rule of mixtures, due to severe shear displacement and strong compositional intermixing along the SB-deformed zone with diffusion of Al into ZrCu layers. Enhanced plastic deformation (> 10%) is observed for Λ = 100 and 200 nm during micropillar compression, but accompanied by a reduction of the yield strength. In contrast, for Λ = 50 nm, deformation is dominated by catastrophic SB events, while the yield strength returns to that of the monolithic films of ~2-2.5 GPa. Our results can be utilized in design of nanostructured metallic glasses with tailored mechanical performance.

Keywords: Thin film metallic glasses; Nanolaminates; Mechanical properties; Micropillar compression; Atom probe tomography.

Metallic glasses (MGs), also known as amorphous metals, exhibit an appealing combination of mechanical properties, such as yield strength and toughness, reaching up to 2 GPa and >80 MPa $m^{1/2}$ for Zr-based compositions, respectively, making them interesting for several applications in the fields of MEMS, micro-gears, biomedical devices and flexible electronics [1-3]. However, the plastic deformation at T_{room} of bulk MGs is highly localized with the formation of shear bands (SBs), leading to catastrophic failure and negligible ductility in tension and limited (up to 2%) plastic deformation in compression [1, 4].

Nevertheless, when the intrinsic size of MG samples is reduced below ~500 nm, as for thin-film MGs (TFMGs), size effects are activated enabling the mitigation of SB localization accompanied by homogeneous plastic deformation [5-7] as shown in micropillar compression tests [5] and tensile tests of freestanding TFMGs [6, 7]. This strategy is often combined with the synthesis of nanolayered architectures that alternate nm-sized crystal and glass sublayers, featuring a high density of interfaces, which further suppress the propagation of SBs, while benefiting from the intrinsic ductility of crystalline layers [8-10]. As an example, Wu *et al.* [10] deposited Cr-Co-Ni (crystalline)/Ti-Zr-Nb-Hf (glass) nanolaminates (NLs) with 10 nm bilayer period, reporting superior yield strength up to 3.6 GPa and significant homogeneous deformation up to ~15% strain in compression without fracture. Studies on fully amorphous NLs also highlight the potential of glass–glass interfaces and local heterogeneities to mitigate catastrophic SBs and enhance the mechanical properties such as yield strength, hardness, and plasticity compared to the monolithic counterparts [11-13]. Chen *et al.* [11] observed high hardness (up to 8.4 GPa) for NiNb/ZrCuNiAl NLs with bilayer period (Λ) of 50 nm, exceeding the value of the rule of mixtures (ROM). Sharma *et al.* [13] performed micropillar compression of fully amorphous Zr-based/La-NL and they reported larger plasticity compared to the monolithic constituents. They resolved SBs confinement within the softer La-based layer which requires higher critical shear stress to penetrate the harder Zr-based sublayers. Recently in Ref. [14], the authors of this study fabricated fully amorphous $Zr_{24}Cu_{76}/Zr_{61}Cu_{39}$ NLs with controlled Λ (from 400 down to 5 nm), with a focus on the SB nucleation and propagation processes, demonstrating extensive chemical

intermixing within SB-deformed regions and a brittle-to-ductile transition when $\Lambda \leq 50$ nm, achieving high yield strength (∼2 GPa) and plastic deformation (∼16%) in compression.

However, investigations into the effect of composition for fully amorphous nanolayered architectures, particularly with the addition of plasticity-enhancing elements such as Al [15, 16], are still lacking. Here, we synthesize fully amorphous ZrCu/$ZrCuAl_9$ NLs with controlled Λ ranging from 200 down to 50 nm using magnetron sputtering, focusing on the evolution of mechanical properties as well as on the propagation of SBs. The $ZrCuAl_9$ layer composition has been selected since it maximizes the density of full and defective icosahedral cluster populations, inducing a more shear-resistant behavior to the material [16]. The mechanical behavior was explored through advanced scale-bridging techniques focusing on both structural and chemical effects of nanointerfaces and Al addition. Our findings demonstrate the activation of significant mechanical size effects, a controlled brittle-to-ductile transition for $\Lambda \geq 100$ nm and notable Al diffusion along SBs, leading to strong interlayer intermixing.

ZrCu/$ZrCuAl_9$ fully amorphous NLs were deposited by magnetron co-sputtering from three (>99.99 % pure) Zr, Cu and Al targets (Kurt J. Lesker®). The base and the deposition pressures were set equal to 10^{-5} and 0.5 Pa, respectively, with an Ar flow rate of 40 sccm at T_{room}. The NLs were fabricated through an automated deposition process by varying the Al target power and controlling the opening/closing of shutters. The power ratio between Zr and Cu targets was calibrated to obtain a $Zr_{50}Cu_{50}$ alloy, while the Al target was periodically switched on/off at 20 W to form $ZrCuAl_9$ [16]. The NLs were deposited on Si (100) substrates with a total film thickness equal to 3200 ± 100 nm, with the soft ZrCu layer always on top. Structural characterization was carried out using a field emission scanning electron microscope (FE-SEM, Zeiss Supra 40) equipped with a Bruker energy dispersive X-ray spectroscopy (EDX), and by X-ray diffraction (XRD, RIGAKU SMARTLAB 9KW) with Cu-Kα (λ = 1.5406 Å) in Bragg–Brentano geometry. The mechanical characterization was performed by nanoindentation using a KLA G200 nanoindenter with a DCM head and diamond Berkovich tip, operating in continuous stiffness measurement (CSM) mode under load control with fixed proportional loading rate of 0.05 s^{-1}. For further details see Ref. [16, 17]. The elastic modulus (E) and hardness (H) were extracted using

the Oliver and Pharr method [18] at indentation depths ~10% of the film thickness with a minimum of 25 indentations performed after calibration on fused silica. The shear ($G = C_{44}$) and longitudinal (C_{11}) elastic moduli were determined by surface Brillouin spectroscopy (SBS), assuming isotropic elasticity of the NL (due to the similar chemistry of the layers) whose effective elastic properties can be directly extracted from the single constituents, see Refs. [14, 19, 20] and Supplementary Information (SI). The stress–strain curves were obtained by compression testing of micropillars, analyzing data for 5 different micropillars per sample, with details in Ref. [14] and the SI. An atom probe tomography (APT) tip was prepared by using focused ion beam (FIB) within a shear band-deformed zone after pillar compression to investigate the 3D elemental distribution locally (more details in the SI).

Figure 1a-c shows the SEM cross-sectional views of the ZrCu/$ZrCuAl_9$ NLs with different bilayer periods (Λ), ranging from 50 (a) up to 200 nm (c), and a total thickness of ~3.2 μm. All specimens exhibit a corrugation pattern on the fracture surface, a characteristic feature of MGs. For specific TFMG compositions, such as ZrCu and ZrCuAl [16], fracture occurs within highly sheared regions of material via a nanoscale "corrugated" mechanism associated with atomic cavitation [21]. Moreover, when the characteristic size of the sample is reduced (i.e. thickness confinement as for TFMGs), the dimension of the veins or corrugations on the fracture surface decreases due to the combined effects of the stress field ahead of the crack tip and the free surfaces [14, 16, 21]. The ZrCu/$ZrCuAl_9$ NLs presented an average corrugation length (thickness direction) that varies with the thickness of each individual layer, ranging from 40 ± 10 up to 150 ± 30 nm, for Λ equal to, respectively, 50 and 200 nm. Notably, larger layer thicknesses promote the formation of larger corrugations, reducing stress confinement ahead the crack tip and facilitating the propagation of SBs during fracture, despite the high density of interfaces. On the other hand, smaller NL thicknesses confine the corrugations, reducing their intrinsic size. Figure 1d presents the XRD diffractograms for the different NLs showing a fully amorphous structure without the presence of nanocrystallites and confirming the full miscibility of Al within the ZrCu alloy. The average interatomic distance, calculated using Ehrenfest equation, is 2.7 Å, similar to what is observed in the literature for $Zr_{50}Cu_{50}$ and $ZrCuAl_9$ MG produced by physical vapor deposition

techniques or by casting [16, 17]. Indeed, the small amount of Al does not shift the position of the broad amorphous diffraction peak, whose variation is on the order of fractions of Å and can only be detected using high-energy diffraction experiments [16].

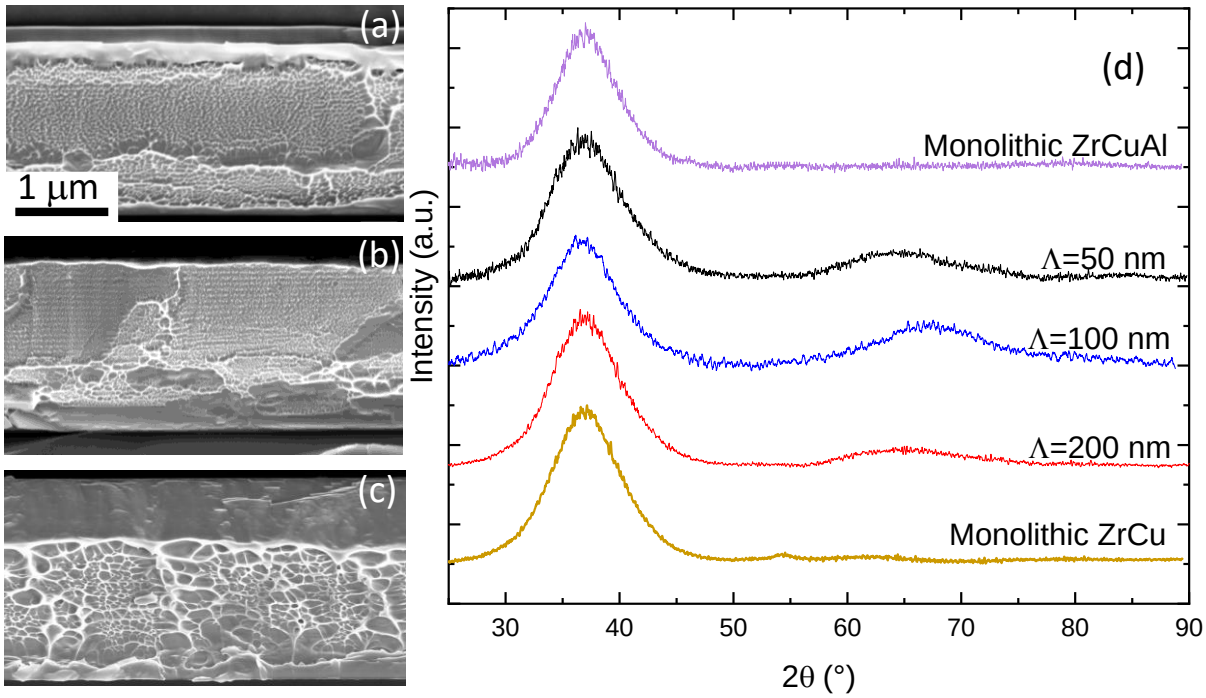

Figure 1 – (a-c) SEM cross-section micrographs of a 3.2 μm-thick ZrCu/$ZrCuAl_9$ NLs with Λ equal to a) 50, b) 100, and c) 200 nm. The different layers can be distinguished with larger corrugation patters for Λ = 200 nm. (d) The corresponding XRD, revealing fully amorphous structure. The monolithic constituent data were taken from Ref. [16].

Figure 2 shows the mechanical characterization results from nanoindentation and SBS. $ZrCuAl_9$ reports a larger elastic and shear elastic modulus (*E* and *G*, respectively) and hardness (*H*) than ZrCu. This is the consequence of the formation of shorter bonds (*i.e.* Al-Zr and Al-Cu) and the strong short range order with a higher fraction of full- and defective icosahedra, which are responsible of the large shear-resistant behavior [16]. For the NL systems, we show that the values of *G* and *E* (Figure 2a,b) are constant for the different Λ, and lie close to the rule of mixture (ROM) calculated from the monolithic constituents ($Zr_{50}Cu_{50}$ and $ZrCuAl_9$), similar to what is observed for the case of $Zr_{61}Cu_{39}/Zr_{24}Cu_{76}$ NLs [14]. This indicates the presence of nearly-perfect interfaces which are sharp and with high interlayer adhesion due to the similar layer chemistry with high fraction of Zr-Cu bonds as already observed in other fully amorphous NLs [13, 14] and discussed later in Fig. 4. Similarly, the *H* values do not depend

on Λ, but they are slightly above the ROM and closer to the harder constituent (*i.e.* $ZrCuAl_9$), even considering that the top layer of the stack is the softer ZrCu. This suggests that the presence of heterogeneities and of sharp nanointerfaces with possible local chemical intermixing [14] compensate the presence of softer top layer, while affecting the plastic zone ahead the indenter tip and thus the *H*. This observation is consistent with $Zr_{24}Cu_{76}/Zr_{61}Cu_{39}$ NLs [14], which, however, showed a much larger hardness variation of ~2.5 GPa between the constituents .

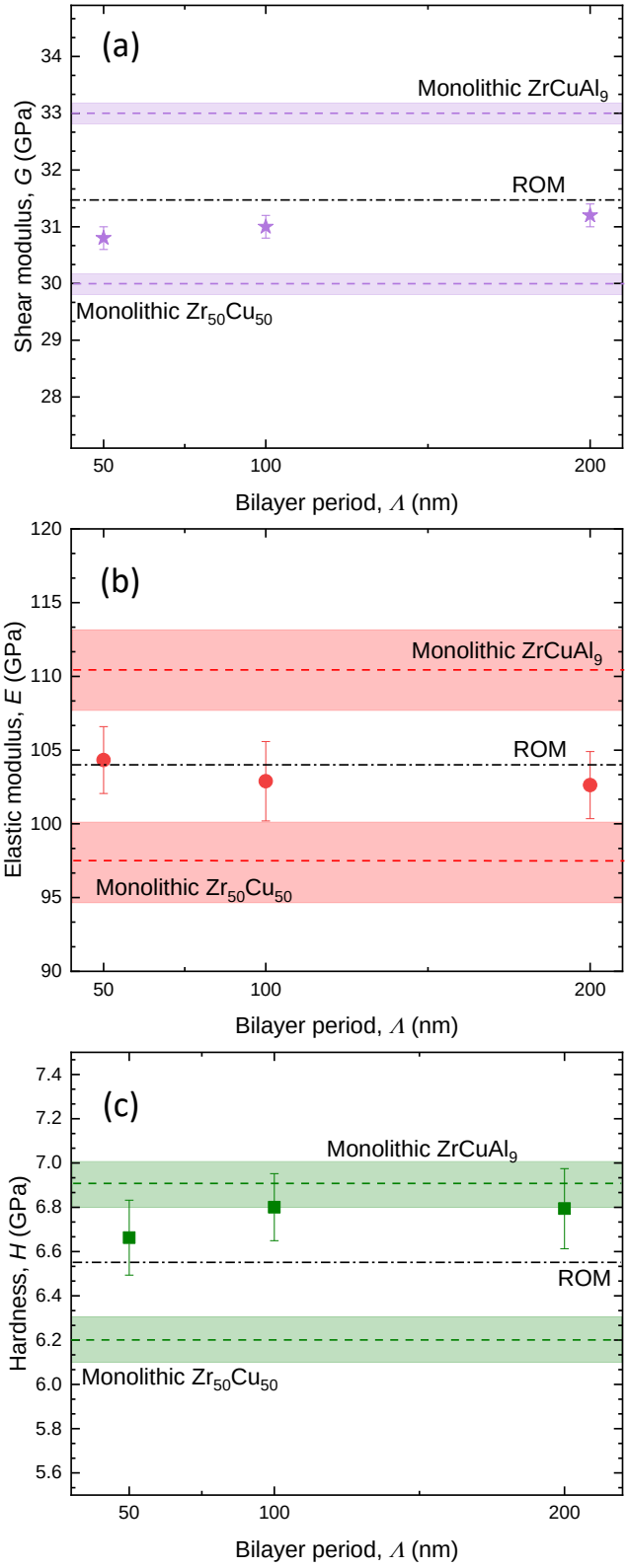

Figure 2 – a) Evolution of shear modulus measured by surface Brillouin spectroscopy and (b) elastic modulus and (c) hardness from nanoindentation for monolith ZrCu and $ZrCuAl_9$ and NLs with different bilayer period (Λ). The values of G and E remain close to the rule of mixture (ROM, black dash-dot lines), while the values of H are higher and close to those of the harder $ZrCuAl_9$. The dashed lines in the graphs represent the values for monolithic reference films (ZrCu and $ZrCuAl_9$) and the shadowed regions represent their respective error bars.

Micropillar compression was performed to investigate the mechanical behavior of fully amorphous NLs under different loading condition (*i.e.*, uniaxial compression) in comparison with nanoindentation, and to investigate the role of periodic heterogeneities on plasticity. Figure 3a presents the results of compression tests for the NLs, compared with the monolithic ZrCu and $ZrCuAl_9$ counterparts. The monolithic films exhibit clear failure through catastrophic SB events upon reaching the yield strength (σ_y), a characteristic feature of MGs [14, 22]. These events are marked by sudden strain bursts in the load-displacement data, as the experiments were performed under load control. This behavior is illustrated in Fig. 3b, which shows the formation of a major SB oriented at ∼45° of the compression direction. The values of σ_y depends on the composition, with the monolithic $ZrCuAl_9$ layer showing a higher value (2.62 ± 0.07 GPa) compared to ZrCu (2.13 ± 0.08 GPa). This increase is attributed to the distinct local atomic order and packing of the Al-containing composition, characterized by a larger content of full icosahedral atomic clusters, leading to greater resistance against shear deformation [16], consistent with nanoindentation results (Fig. 2).

In the NLs with Λ = 50 nm, the mechanical behavior remains brittle, with failure occurring upon yielding (blue curve in Figure 3a). This brittleness can be explained by the lower thickness of the harder $ZrCuAl_9$ layer, resulting in a reduced blocking effect of SBs propagation. Additionally, smaller bilayer periods result in less sharp and distinct interfaces, promoting the nucleation of SBs upon yielding, as reported in Ref. [14]. Finally, for very fine NLs, the overall structure of the stack mechanically behaves as a monolithic material. This is due to the very similar chemistry between ZrCu and $ZrCuAl_9$, as well as to the small mechanical contrast between these layers (hardness variation = ∼0.6 GPa, Fig. 2), reducing their effectiveness as barriers against SB propagation and resulting in a value of σ_y (2.01 ± 0.10 GPa) similar to the softer ZrCu layers. Such behavior is very different from micropillar compression tests of $Zr_{24}Cu_{76}/Zr_{61}Cu_{39}$ NLs with the same bilayer period, reporting extended plasticity but stronger chemical contrast and hardness variation (∼2.5 GPa) between the layers, Ref. [14], highlighting how mechanical performance are significantly connected with both chemistry and NL architecture.

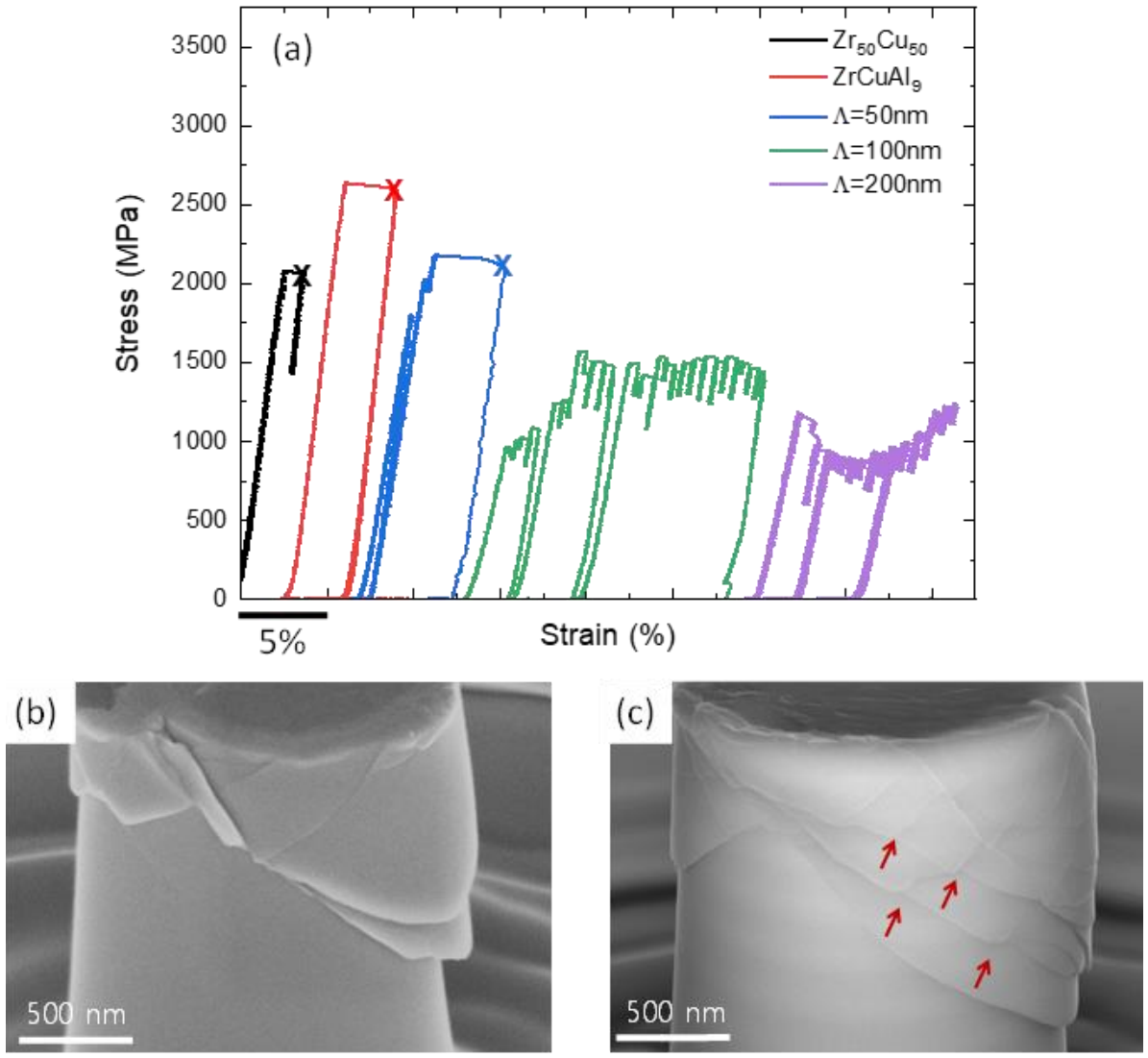

Figure 3 – a) Stress-strain curves of monolithic and multi-layered ZrCu/$ZrCuAl_9$ TFMGs. The "X" corresponds to a catastrophic failure event. b,c) *Post-mortem* SEM micrographs of micropillars after compression showing (b) typical failure of monolithic (ZrCu) films with the propagation of a major SB event and (c) the formation of multiple SBs and deviation and stopping phenomena (red arrows) observed in Λ = 200 nm NLs .

On the other hand, the mechanical behavior completely changes for $\Lambda > 50$ nm (green and purple curves in Fig. 3a), with a substantial reduction of σ_y down to 0.94 ± 0.03 and to 1.14 ± 0.04 GPa for Λ = 100 and 200 nm, respectively. However, this reduction of σ_y is accompanied by smaller strain bursts, avoiding catastrophic failure up to strain values of ~15 %. The reduction of σ_y is attributed to either the presence of sharper interfaces promoting SBs nucleation (which are originated at free volume-rich regions) and/or to the presence of softer ZrCu layers (especially on top of the stack), similar to what was observed in Ref. [14]. Due to the extremely fast and stochastic nature of SB events,

it is not possible to definitively determine whether they nucleate from the external surface, the interfaces, or the lower shear resistance ZrCu layers, which are located on the top layer and in contact with flat punch counterbody. However, larger Λ could effectively hinder the propagation of SBs as a result of the presence of sharper interfaces and thicker and more shear-resistant $ZrCuAl_9$ layers [16], despite the smaller mechanical contrast between the layer constituents. This is also supported by the *post mortem* analysis of the micropillars showing the presence of multiple SBs events which have limited percolation (red arrows in Fig. 3c). This can explain the presence of discrete stress increments in the stress–strain curves for such NLs as shown in Figure 3a. Finally, the increment of stress at higher deformations for NLs with Λ = 200 nm is related to the increment of the load-bearing cross-sectional area during compression due to the multiple SB activation.

APT specimen extracted from a *post-mortem* deformed micropillar enables the investigation of deformation processes, providing in-depth information on the chemical evolution induced by the interaction between SBs and the heterogeneities of the NLs structure (Figure 4). The SB has a characteristic width of ~10 nm, which aligns with the reported values in literature for Zr-based MGs [23]. Its propagation through the layers results in severe local deformation, similarly to what was observed in Ref. [14], indicating the ability of the NL to sustain plasticity through the deformation of its individual layers. Moreover, the propagation of SBs leads to a misalignment of the original layer stack and result in the presence of Al within the ZrCu layer and its depletion within the $ZrCuAl_9$ layer. This displacement by shear is also accompanied by the interdiffusion phenomena mediated by the temperature rise in SB process and the activation of shear transformation zones (STZs) [14].

These effects are shown in the 2D contour plot for Al (Figure 4a) and the 1D concentration profiles across the SB path (Figures 4b,c), indicating localized chemical intermixing and the presence of Al within the SB and in the ZrCu layer, while highlighting a negligible O (and other impurities) content. In our previous work Ref. [14], we reported shear displacement and local intermixing phenomena in fully amorphous $Zr_{24}Cu_{76}$ and $Zr_{61}Cu_{39}$, leading to average $Zr_{50}Cu_{50}$ composition in the SB-deformed zone. Here, we report significant presence of Al along the SB as a result of the shear displacement in

combination with the compositional gradient across the layers and the activation of STZs, which induce appreciable atomic rearrangement between adjacent amorphous nanodomains, facilitating homogenization rather than phase separation toward equilibrium, as reported inside some SBs [24]. These phenomena can also be boosted by potential local heating effects during SB propagation, which may result in localized temperature increments approaching or exceeding the melting temperature, thereby promoting interdiffusion [25, 26]. Finally, Figure 4d highlights the presence of local compositional oscillations of ~±10 at. % within 2-3 nm for ZrCu and ~±2-3 at. % Al in $Zr_{50}Cu_{40}Al_{10}$ layer (film growth direction), while reporting the presence of very thin interface (~2-3 nm) between the ZrCu and the $ZrCuAl_9$ layer in which a small chemical gradient can be detected. Such chemical fluctuations are results for the extreme out-of-equilibrium condition of sputtering, resulting in nm-scale compositional fluctuations which minimize the energy of (meta)stable TFMGs, similar to what is reported in Ref. [27] for ZrCu TFMGs deposited by PLD. Interestingly, such compositional oscillations mitigate during SB propagation as a results of local intermixing (Figure 4b,c). Finally, since these fluctuations occur on a ~2-3 nm scale, we can assume a negligible contribution to the measured average mechanical properties (nanoindentation and micropillar compression), as these techniques probe a larger volume. Furthermore, because the monolithic layer constituents (ZrCu and ZrCuAl) were produced using identical deposition parameters, the evolution of the mechanical properties are primarily dictated by the thickness/chemistry of the sublayers and the interface density.

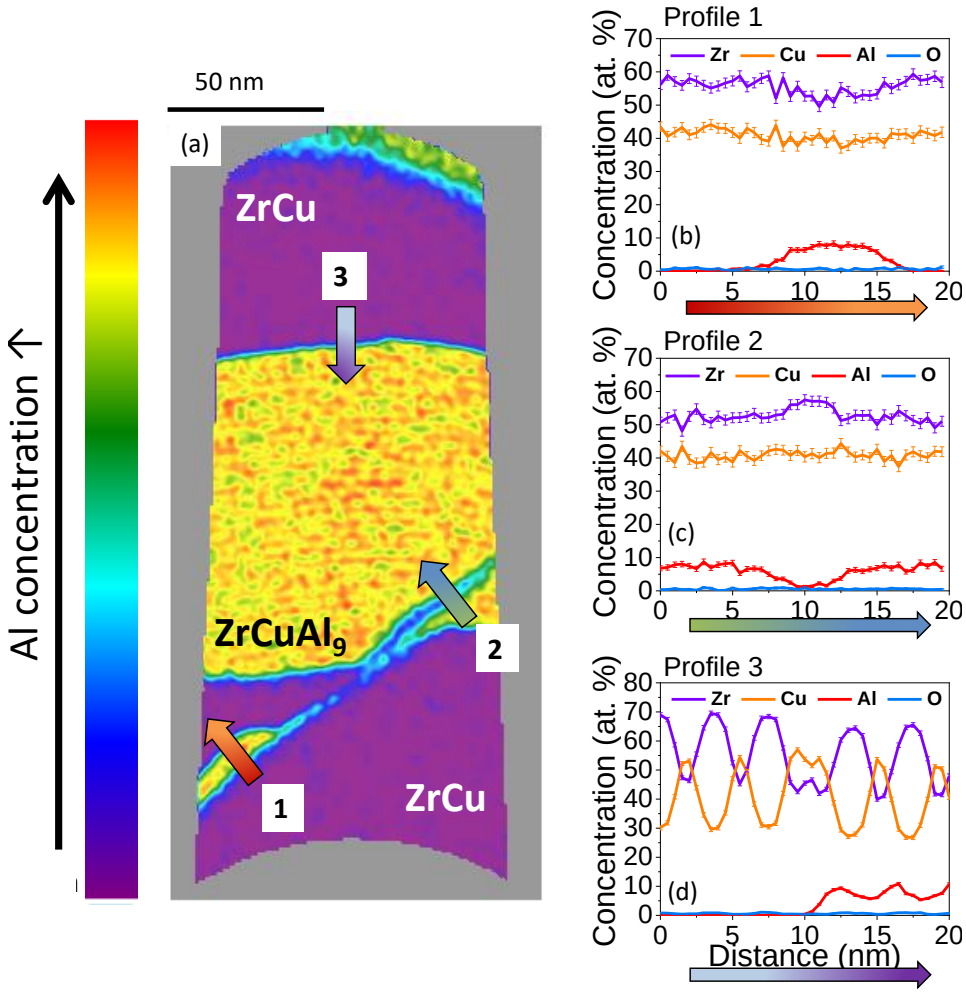

Fig. 4 – *Post-mortem* chemical analysis of 3 µm thick ZrCu/ZrCuAl$_9$ NL with Λ = 200 nm after micropillar compression. The 2D contour plot of Al (a) and the 1D concentration profiles (*i.e.*, within cylindrical regions of interest of Φ4 × 20 nm) of two different positions across the SB path indicated by arrows (1) and (2) (b,c) and across the ZrCu/ZrCuAl$_9$ interface indicated by the arrow (3) (d). Color gradients highlight the large chemical intermixing and possible Al diffusion between the layers.

In conclusion, we fabricated fully amorphous ZrCu/ZrCuAl$_9$ nanolayers (NLs) with different bilayer periods (Λ), with tailored mechanical properties and deformation mechanism governed by the chemistry/thickness of the sublayer and density o interfaces. Specifically:

- For large sublayer thicknesses (Λ = 100 and 200 nm) multiple SBs tend to nucleate either from the interfaces or from the low shear resistant and thick ZrCu layer. However, these SBs do not percolate through the entire micropillar due to the blocking effects of subsequent interfaces and the presence of thick higher shear resistance ZrCuAl layers. This explains the lower yield strength accompanied by

a reduced serration flow, while preventing catastrophic failure within a single SB event even for deformations >10%.

- For small bilayer thicknesses (Λ = 50 nm) the mechanical behavior resembles that of a monolithic counterpart due less sharp and distinct interfaces with thin ZrCuAl layers which being less effective at blocking SB propagation upon yielding. This leads to mechanical behavior similar to monolithic films, characterized by yield strength close to pure ZrCu and catastrophic failure with the propagation of a single SB.

Moreover, we observed significant compositional variations within the SB-deformed zones (Al presence into the ZrCu layers), as a result of shear displacement between layers accompanied by local diffusion, while explaining the evolution of the mechanical behavior as a result of layer intermixing, severe local deformation processes and the presence of nanointerfaces. Overall, we demonstrate how controlling structural and chemical heterogeneities through the fabrication of fully amorphous nanolaminates (NLs) opens up new possibilities with interest for their application particularly in the field of micro and flexible electronics and of structural coatings.

Acknowledgements

M. Ghidelli acknowledges the financial support of the ANR "MICRO-HEAs" (grant agreement no. ANR-21-CE08-0003-01) as well as of the ANR "EGLASS" (grant agreement no. ANR-22-CE92-0026-01). M. Ghidelli and C. Poltronieri acknowledge the financial support of Partenariats Hubert Curien (PHC) PROCOPE 2021 project ''New-Glasses" (Grant #46735ZG) financing the cooperation between LSPM and MPIE. J.P. Best and A. Brognara acknowledge the Deutsche Akademische Austauschdienst (DAAD) within program "Programme des projektbezogenen Personenaustauschs (PPP)" (Project-ID: 57561649) financed by the Bundesministerium für Bildung und Forschung (BMBF). C. Jung acknowledges the Global Joint Research Program funded by Pukyong National University (202411890001).

Declaration of competing interest

The authors declare that they have no known competing financial interests or personal relationships that could have appeared to influence the work reported in this paper.

References

[1] C.A. Schuh, T.C. Hufnagel, U. Ramamurty, Mechanical behavior of amorphous alloys, Acta Mater. 55 (2007) 4067-4109.

[2] J.J. Lewandowski, W.H. Wang, A.L. Greer, Intrinsic plasticity or brittleness of metallic glasses, Philos. Mag. Lett. 85 (2005) 77-87.

[3] M. Telford, The case for bulk metallic glass, Mater. Today 7 (2004) 36-43.

[4] A.L. Greer, Y.Q. Cheng, E. Ma, Shear bands in metallic glasses, Mater. Sci. Eng., R 74(4) (2013) 71-132.

[5] J.R. Greer, J.T.M. De Hosson, Plasticity in small-sized metallic systems: Intrinsic versus extrinsic size effect, Prog. Mater. Sci. 56 (2011) 654-724.

[6] M. Ghidelli, H. Idrissi, S. Gravier, J.-J. Blandin, J.-P. Raskin, D. Schryvers, T. Pardoen, Homogeneous flow and size dependent mechanical behavior in highly ductile Zr65Ni35 metallic glass films, Acta Mater. 131 (2017) 246-259.

[7] H. Guo, P.F. Yan, Y.B. Wang, J. Tan, Z.F. Zhang, M.L. Sui, E. Ma, Tensile ductility and necking of metallic glass, Nature Mater. 6(10) (2007) 735-9.

[8] J.-Y. Kim, D. Jang, J.R. Greer, Nanolaminates Utilizing Size-Dependent Homogeneous Plasticity of Metallic Glasses, Adv. Fun. Mater. 21(23) (2011) 4550-4554.

[9] W. Guo, E. Jägle, J. Yao, V. Maier, S. Korte-Kerzel, J.M. Schneider, D. Raabe, Intrinsic and extrinsic size effects in the deformation of amorphous CuZr/nanocrystalline Cu nanolaminates, Acta Mater. 80 (2014) 94-106.

[10] G. Wu, C. Liu, A. Brognara, M. Ghidelli, Y. Bao, S. Liu, X. Wu, W. Xia, H. Zhao, J. Rao, D. Ponge, V. Devulapalli, W. Lu, G. Dehm, D. Raabe, Z. Li, Symbiotic crystal-glass alloys via dynamic chemical partitioning, Mater. Today 51 (2021) 6-14.

[11] Z. Chen, M. Li, J. Cao, F. Li, S. Guo, B. Sun, H. Ke, W. Wang, Interface dominated deformation transition from inhomogeneous to apparent homogeneous mode in amorphous/amorphous nanolaminates, Journal of Materials Science & Technology 99 (2022) 178-183.

[12] S. Kuan, H. Chou, M. Liu, X. Du, J. Huang, Micromechanical response for the amorphous/amorphous nanolaminates, Intermetallics 18(12) (2010) 2453-2457.

[13] P. Sharma, K. Yubuta, H. Kimura, A. Inoue, Brittle metallic glass deforms plastically at room temperature in glassy multilayers, Physical Review B—Condensed Matter and Materials Physics 80(2) (2009) 024106.

[14] A. Brognara, A. Kashiwar, C. Jung, X. Zhang, A. Ahmadian, N. Gauquelin, J. Verbeeck, P. Djemia, D. Faurie, G. Dehm, H. Idrissi, J.P. Best, M. Ghidelli, Tailoring Mechanical Properties and Shear Band Propagation in ZrCu Metallic Glass Nanolaminates Through Chemical Heterogeneities and Interface Density, Small Struct. (2024) 2400011.

[15] J. Das, M.B. Tang, K.B. Kim, R. Theissmann, F. Baier, W.H. Wang, J. Eckert, ‘‘Work-Hardenable’’ Ductile Bulk Metallic Glass, Phys. Rev. Lett. 94 (2005) 205501.

[16] C. Poltronieri, A. Brognara, F. Bignoli, S. Evertz, P. Djemia, D. Faurie, F. Challali, C. Li, L. Belliard, G. Dehm, J.P. Best, M. Ghidelli, Mechanical properties and thermal stability of ZrCuAlx thin film metallic glasses: Experiments and first-principle calculations, Acta Mater. 258 (2023) 119226.
[17] A. Brognara, J.P. Best, P. Djemia, D. Faurie, G. Dehm, M. Ghidelli, Effect of composition and nanostructure on the mechanical properties and thermal stability of Zr100-xCux thin film metallic glasses, Mater. Design 219 (2022) 110752.
[18] W.C. Oliver, G.M. Pharr, Measurement of hardness and elastic modulus by instrumented indentation: Advances in understanding and refinements to methodology, J. Mater. Res. 19 (2003) 3-20.
[19] M. Grimsditch, Effective elastic constants of superlattices, Phys. Rev. B 31(10) (1985) 6818.
[20] S. Rytov, Acoustical properties of a thinly laminated medium, Sov. Phys. Acoust 2(1) (1956) 68-80.
[21] M. Ghidelli, S. Gravier, J.-J. Blandin, J.-P. Raskin, F. Lani, T. Pardoen, Size-dependent failure mechanisms in ZrNi thin metallic glass films, Scripta Materialia 89 (2014) 9-12.
[22] D. Tonnies, R. Maass, C.A. Volkert, Room temperature homogeneous ductility of micrometer-sized metallic glass, Adv. Mater. 26(32) (2014) 5715-21.
[23] Y. Zhang, A.L. Greer, Thickness of shear bands in metallic glasses, Appl. Phys. Lett. 89 (2006) 071907.
[24] S. Balachandran, J. Orava, M. Köhler, A.J. Breen, I. Kaban, D. Raabe, M. Herbig, Elemental re-distribution inside shear bands revealed by correlative atom-probe tomography and electron microscopy in a deformed metallic glass, Scripta Mater. 168 (2019) 14-18.
[25] J.J. Lewandowski, A.L. Greer, Temperature rise at shear bands inmetallic glasses, Nature Mater. 5 (2006) 15-18.
[26] K.S. Nakayama, Y. Yokoyama, G. Xie, Q.S. Zhang, M.W. Chen, T. Sakurai, A. Inoue, Metallic Glass Nanowire, Nano Lett. 8 (2007) 516-519.
[27] M. Ghidelli, A. Orekhov, A.L. Bassi, G. Terraneo, P. Djemia, G. Abadias, M. Nord, A. Béché, N. Gauquelin, J. Verbeeck, J.-P. Raskin, D. Schryvers, T. Pardoen, H. Idrissi, Novel class of nanostructured metallic glass films with superior and tunable mechanical properties, Acta Mater. 213 (2021) 116955.